eTransportation 11 (2022) 100148

Contents lists available at ScienceDirect

eTransportation

journal homepage: www.journals.elsevier.com/etransportation

Combustion characteristics of lithium–iron–phosphate batteries with different combustion states

Q.I. Peiyan [a], Zhang Ming Jie [b], Jiang Da [c], Yang Kai [b, **], Li Jianling [a, *], Lai Yilin [b], Gao Fei [b], Liu Hao [b]

[a] State Key Laboratory of Advanced Metallurgy, School of Metallurgical and Ecological Engineering, University of Science and Technology Beijing, Beijing, 100083, China
[b] State Key Laboratory of Operation and Control of Renewable Energy &, Storage Systems, China Electric Power Research Institute, Beijing, 100192, China
[c] State Grid Jiangsu Electric Vehicle Service Company, Ltd. Nanjing, 210019, China

ARTICLE INFO

Article history:
Received 30 August 2021
Received in revised form
30 November 2021
Accepted 1 December 2021
Available online 6 December 2021

Keywords:
$LiFePO_4$ cell
Fire behaviors
Thermal runaway
Gas release
Firefighting and protective measures

ABSTRACT

The lithium-ion battery combustion experiment platform was used to perform the combustion and smouldering experiments on a 60-Ah steel-shell battery. Temperature, voltage, gases, and heat release rates (HRRs) were analysed during the experiment, and the material calorific value was calculated. The results showed that the highest surface temperatures are 323 and 331.4 °C, respectively. The combustion states did not affect the severity of thermal runway inside the battery. Battery combustion exhibited a high thermal hazard, and its total heat release was approximately 17 times that of the smouldering process. The smouldering process showed a high gas hazard. The toxic gas concentration in this experimental platform (6.48 m^3) can reach 5.38 times the lethal concentration. The HRR and remaining energy of the battery were greatly affected by the combustion states. The proportion of energy remaining under the smouldering states was as high as 75.8% after the test.

1. Introduction

With the commercialisation of lithium-ion batteries (LIBs), battery safety has gained increasing attention. In recent years, battery fires and explosions, such as the explosions of Samsung and Apple mobile phones, burning of BYD taxis, and the spontaneous combustion of Tesla electric car batteries, have been reported at times [1].

As an energy-containing system, LIBs cause immeasurable damage to the equipment, operator, and environment when an accident occurs. All safety accidents of LIBs are accompanied by internal and external short circuits, leading to a rapid temperature increase. Then, the exothermic reaction becomes uncontrollable, and a large amount of energy and pressure accumulate in the battery until the safety valve breaks [2–4].

Thermal runaway (TR) is the main cause of accidents in LIBs. Many studies have explained the TR mechanism. The reactions in the TR process [5] usually include solid electrolyte interface (SEI) film decomposition [6], separator melting [7,8], reactions between the electrode and electrolyte [9,10], and electrolyte decomposition [11]. These reactions cause and control the burning behaviour of LIBs.

In addition, the fire emissions of LIBs contain many toxic gases, such as CO, H_2, and HF [12–15]. These combustible and toxic gases spread rapidly, and when they spread to crowded places, they are likely to cause mass poisoning. Therefore, the assessment of the gas toxicity is also an important aspect of fire risk.

Various studies have been conducted on fire behaviours. Most experiments have studied the combustion characteristics of batteries in terms of state of charge (SOC) [16–19], capacity [20,21], and TR triggering methods [18]. Few studies have focused on different combustion states.

In practical applications, batteries generally have three combustion states: flame burning, flameless smouldering, and explosion. Understanding the combustion characteristics and fire hazards of batteries under different combustion states can provide a certain reference for the firefighters when dealing with accidents and is considerably important for the subsequent targeted implementation of firefighting and protective measures.

* Corresponding author.30 Xueyuan Road, Haidian District, Beijing, China
** Corresponding author.15 Xiaoying East Road, Qinghe, Haidian District, Beijing, China
E-mail addresses: ykbit@126.com (Y. Kai), lijianling@ustb.edu.cn (L. Jianling).

https://doi.org/10.1016/j.etran.2021.100148
2590-1168/

In this paper, battery TR is triggered with a 500-W heating plate, and several parameters of LIBs, such as temperature, voltage, gas release, and heat release rate (HRR), are measured during flame combustion and flameless smouldering experiments. The energy changes of the battery system are calculated. The battery fire hazard is evaluated by analysing the combustion characteristics of LIBs in different combustion states. The experimental conclusions can provide reference basis for firefighters to implement firefighting and safety protection strategies.

2. Experimental

2.1. Battery samples

The batteries employed are a 60-Ah large-format LIB with a $LiFePO_4$ (LFP) cathode and a carbon-based anode. The electrolyte used is the solution of a lithium salt ($LiPF_6$) and a mixture of organic solvents, containing ethylene carbonate, dimethyl carbonate, and methyl carbonate. The separator is PP/PE/PP material. The nominal voltage is 3.2 V. The length, width, and height (without considering the tab height) of the battery are 209, 28, and 138 mm, respectively. A safety valve is installed on the top of the cell. The burst pressure of the safety valve is 0.8 MPa. Two cells were pre-cycled with a constant current and constant voltage to 100% SOC before the experiment, and then, were numbered as LFP-1 and LFP-2.

2.2. Experimental apparatus

Fig. 1 presents the schematic diagram of the experimental system. The apparatus comprises four main subsystems to analyse battery voltage, temperature, gases, and HRR. CO, CO_2, H_2, and HF were quantitatively analysed using Fourier transform infrared spectroscopy. A high-definition camera was fixed at the observation window outside the combustion chamber to record the test phenomenon.

The battery was heated using a custom 500-W heating plate. The battery and heating plate were wrapped with high-temperature-insulation cotton to reduce heat dissipation. The stainless steel clamps were used to clamp them, and they were squeezed with stones. A data recorder was used to record the temperature and voltage changes of the cell during combustion. The heating plate was turned off when the battery voltage dropped below 3 V for the first time.

In the pre-experimental process, the 100% SOC battery did not self-ignite under ventilated states, but only smoke spewed out. Therefore, an electric ignition device was used to ignite the flammable gases. Location of igniter is shown in Fig. 1. During the experiment, the electric igniter was always kept on so that the combustible gas could ignite immediately after the safety valve ruptured to minimise the impact on the HRR measurement.

Fig. 2 shows the thermocouple setup. Seven K-type thermocouples, namely TC_1—TC_7, were fixed onto the shell of battery and flame position above the battery to measure temperatures. TC_6 and TC_7 thermocouples were set up 10 and 30 cm above the battery safety valve.

The Pair6400 oxygen bomb calorimeter was used to measure the combustion heat value. The sample was burned in a high-pressure oxygen environment during the experiment. The combustion heat value of the sample was calculated by recording the temperature change and comparing it with the combustion heat value of the standard material. Before the experiment, a new cell was disassembled, and the combustion heat value of its each material was measured, and then, the theoretical exotherm of the combustion process was estimated. This theoretical exotherm was based on the mass ratio between the materials. The cell was ground to measure combustion heat after the experiment, and the remaining energy of the battery was calculated.

3. Results and discussion

3.1. Combustion behaviours

Fig. 3 presents the typical burning behaviour with time for different stages of the battery.The combustion behaviour of batteries in different combustion states is similar (Fig. 3).

Stage I (preheating or venting): The first stage was from the beginning of heating to the rupture of the safety valve, which is the energy accumulation stage. During this process, many chemical and physical reactions occurred in LIBs. As the temperature increased, LFP-1 and LFP-2 produced a small amount of white smoke at 673 and 626 s, respectively, due to the ablation of the insulation wool and high-temperature tape with the heating plate. The internal pressure of LFP-1 and LFP-2 reached the bursting limit of the safety valve, 0.8 MPa, at 1059 and 985 s, respectively. Subsequently, the safety valve ruptured and a large amount of white smoke was ejected, and the concentration of the gases (CO_2, CO, HF, and H_2) to be tested in the experiment considerably increased. The white smoke was mainly a mixture of electrolyte vapour, carbon oxide, and hydrocarbons [13].

Stage II (stable combustion): With the opening of the safety valve, the cell changed from a closed system to an open system. At this stage, in the LFP-1 combustion experiment, combustible gas ignited through the external igniter and presented a stable combustion. LFP-2 smoldering experiment kept smoking without an external igniter, but the amount of gas was not large. Stage II of the two batteries lasted for 136 and 116 s.

Stage III (violent burning or smoking): As the battery temperature continued to increase, the internal separator of the battery melted and caused an internal short circuit (ISC). Then, the battery entered an irreversible TR process. When TR occurred, a considerable amount of heat was accumulated and released in a short time span. At this stage, LFP-2 with the smouldering process was manifested as violent smoking behaviour. However, the violent combustion behaviour of LFP-1 was manifested as multiple jet fires. LFP-1 and LFP-2 lasted for 179 and 201 s, respectively, in this stage, and two jet fires were observed in LFP-1, which lasted for 16 and 22 s. At 1165 s, a large amount of gas produced by LFP-2 filled the entire combustion chamber, resulting in zero visibility.

Stage IV (weakening and extinguishing): During this stage, the release of gases continually decreased, and the flame gradually weakened with the consumption of materials inside the battery. LFP-1 and LFP-2 lasted for 805 and 848 s, respectively, in this stage.

3.2. Temperature variations

The safety valves of LFP-1 and LFP-2 ruptured after heating for 1059 and 985 s, respectively (Fig. 4). Before the cracking of the safety valve, surface temperatures showed the same rate of increase, except for point TC2 of the safety valve, which was attributed to the heating plate. The temperature measurement point (TC2) situated at the battery safety valve was closer to the flame, which was more susceptible to heat radiation from the flame than other three temperature measurement points (TC3—TC5) located on the back of the battery. The fire releases a large amount of heat; however, most of this heat is not utilised to heat the cell [22]. Therefore, the average value of TC3—TC5 can be considered the temperature change of the battery. As shown in Fig. 5, the temperature maximum values of LFP-1 and LFP-2 are 323 and 331.4 °C, respectively. After safety valve cracking, the gas of LFP-1 was ignited with the igniter, and the flame temperature instantly

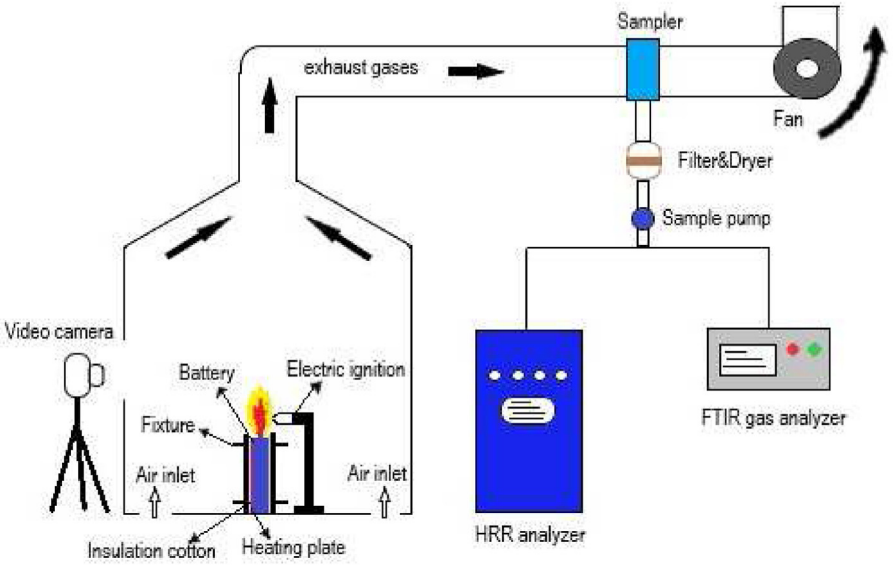

Fig. 1. Schematic diagram of the lithium ion battery burning test apparatus.

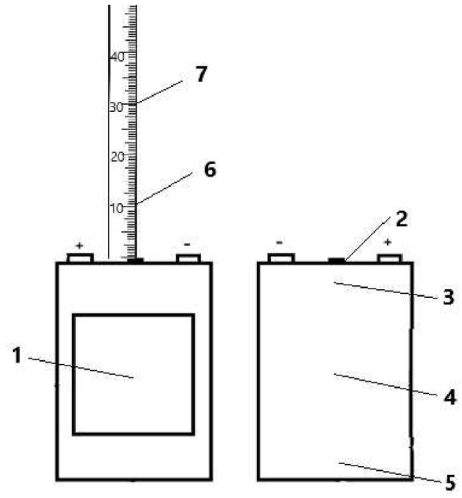

Fig. 2. The thermocouples set up during the experiments.

reached over 820 °C. The gas temperature of LFP-2 could be up to 141.1 °C. In addition, TC1 of both the batteries decreased rapidly after the safety valve ruptured due to the decrease in the internal pressure of the battery after the high-temperature gas ejected, which made the thermocouple to stop clinging to the heating plate. The voltage of the two batteries dropped to 0 V approximately 200 s after the safety valve ruptured, and then, the surface temperatures of the battery began to increase instantly, showing that many violent exothermic reactions occurred simultaneously inside the battery.

The temperature on the side of the battery presented hysteresis, and the internal reaction of the battery could not be expressed in real time. To determine the lag time of the side temperature of the battery, the TR trigger node is set to a temperature rise rate of 1°C/s, and an internal short circuit occurs at the same time. As shown in Fig. 5(a), the TR trigger node of LFP-1 appears at 1382 s. At this time, the battery surface heating rate is 1°C/s, which continues to increase. The ISC of LFP-1 triggers the node at 1195 s (Fig. 4(a)); hence, the lag time is 187 s. Similarly, the ISC of LFP-2 occurs at 1101s, the

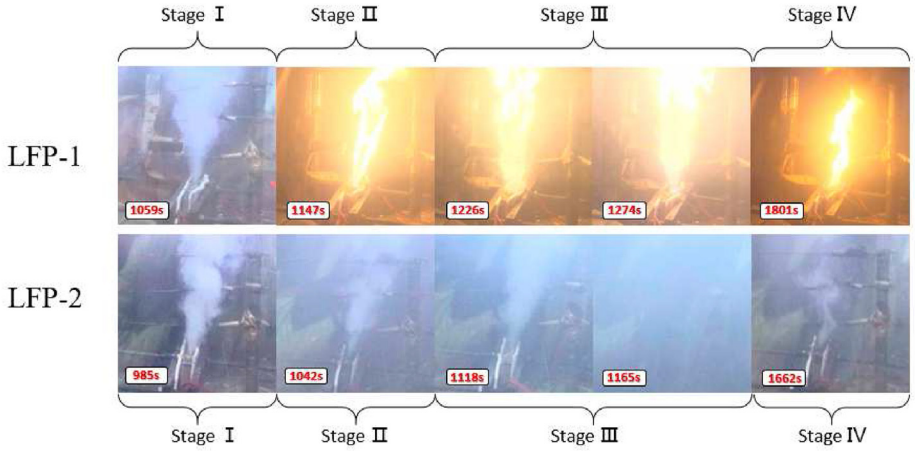

Fig. 3. Combustion behaviors of smoldering and burning LIBs.

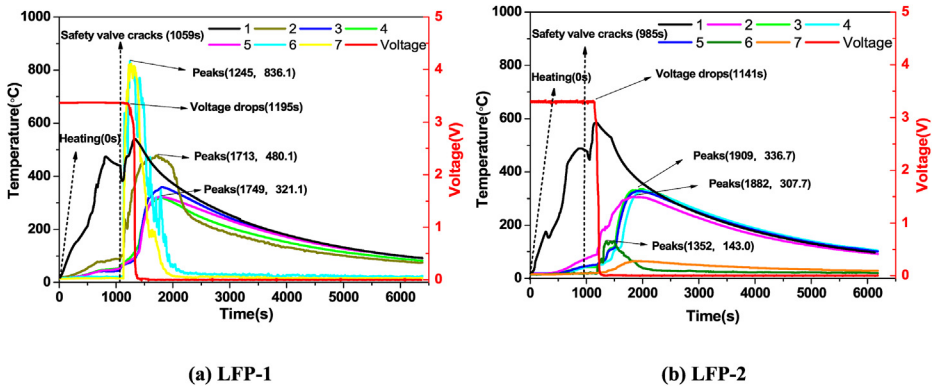

Fig. 4. Temperature curves of LIBs in different combustion states.
(a) Flaming combustion, (b) Flameless smoldering.

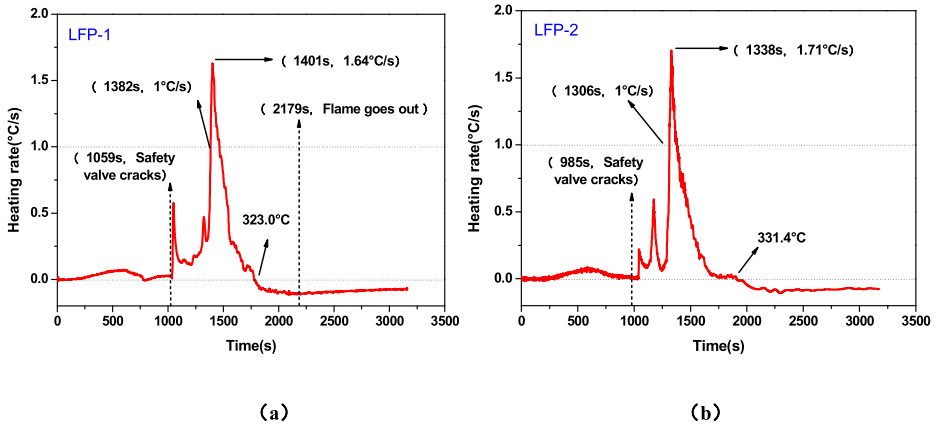

Fig. 5. Heating-rate curve of battery surface.

TR trigger node is 1306 s, and the lag time is 205 s. Specific information is presented in Table 1.

When TR occurred, temperature on the surface of LFP-1 and LFP-2 was 109.6 °C and 102.9 °C, respectively. The highest heating rate was 1.64 °C/s and 1.71 °C/s, respectively; their duration of TR was 89 s and 82 s, respectively. These results showed that the combustion states did not affect the severity of TR inside the battery. It can be seen that the TR trigger temperature measured by the experiment is lower than the experimental results (138~147 °C) measured by accelerating rate calorimeter(ARC) in the literature [2,23,27]. This is because the method used by ARC is a "heating-waiting-searching" cycle, and the internal heat of the battery could be completely released. This experiment involved a continuous heating method. A large temperature difference exists between the internal and surface temperatures of the battery.

3.3. Heat release rate

HRR is a basic parameter that affects fire development and reflects the change in the intensity of heat release of the fire [24]. The total energy value of combustion and change in energy release with time could be obtained through the HRR profile. The HRR test system is used to calculate HRR with the oxygen consumption principle, and the energy produced by consuming a unit mass of oxygen is 13.1 MJ/kg. Fig. 6 shows the relationship between HRR and the time of the battery under different combustion states and indicates that the total heat release (THR) of LFP-1 was 17 times higher than that of LFP-2. The combustion heat was calculated by integrating the HRR curve. In addition, a part of battery heat was released by Joule heat and the internal exothermic chemical reaction. The HRR curve was divided into four stages : The preheating stage (S1), stable burning or smoking stage (S2), violent burning or smoking stage (S3), and weakening and extinguishing stage (S4). S2 and S3 were distinguished by considering the start to decline of the voltage as the node.

No obvious phenomenon was observed before the safety valve ruptured at S1; thus, the HRR value was always zero. The first HRR peak of LFP-1 resulted from the gas accumulated at the preheating stage before combustion; then, the gas was ignited at the beginning of S2. The values of the second HRR peak corresponded to jet fire.

Table 1
Detailed information about feature node of LIBs in different combustion states.

	ISC node(s)	TR node(s)	lag time(s)	TR temperature(°C)	TR duration(s)
LFP-1	1195	1382	187	109.6	89
LFP-2	1101	1306	205	102.9	82

Fig. 6 shows that the values of the second HRR peak were slightly lower than those of the first HRR peak because the jet fire of LFP-1 burnt incompletely and was accompanied by a large amount of jet smoke [25]. Only one HRR peak was observed during the smouldering experiment without the flame effect. The maximum HRR values of LFP-1 and LFP-2 were 37.9 and 2.4 kW, respectively. Detailed information is presented in Table 2.

The calculation of heat release at each stage is shown in Table 3. The heat release of cells was the highest in S3 due to ISC and a voltage drop. Simultaneously, the internal system of the battery began to collapse, a large amount of Joule heat accelerated battery TR, and the battery temperature commenced to increase rapidly. Both LFP-1 and LFP-2 attained the maximum temperature increase rate at S3. However, the temperature of TC3−TC5 did not start to rise rapidly until S4 due to the heat transfer hysteresis. Most combustible materials inside the battery at S3 were consumed, and the flame and smoke gradually weakened at S4.

3.4. Gas analysis

LIBs are energy-storage systems, and all the materials in them such as the electrolyte and separator are organic compounds. Toxic substances such as CO, HF, and aldehydes may be leaked with an accident, which can cause harm to people and the environment. The gases we studied in this paper are CO_2, CO, HF, and H_2. The variations in gases during the experiment under different combustion states are shown in Fig. 7.

The concentration of each gas increased rapidly after the safety valve ruptured (Fig. 7). These gases were mainly generated by SEI layer decomposition [6,26], electrolyte decomposition [27–29], and the reaction between the organic solvent and lithium inserted in the negative electrode [9,30].

Due to the flame of the LFP-1 combustion process, some combustible gases (CO, H2) and combustible materials inside the battery were consumed. Therefore, LFP-1 produced more CO_2 than LFP-2. By contrast, the output of CO and H_2 of LFP-2 was relatively large. The output of HF of LFP-1 was relatively lower may be because of two reasons: 1. The water vapour generated through the combustion of organic solvents, such as electrolytes, absorbs a part of HF and forms acidic substances attached to the battery surface. 2. The degree of reaction between the electrolyte and organic solvent is different.

CO and HF produced through battery combustion are toxic gases. Investigations showed that 85% of deaths in fires are caused

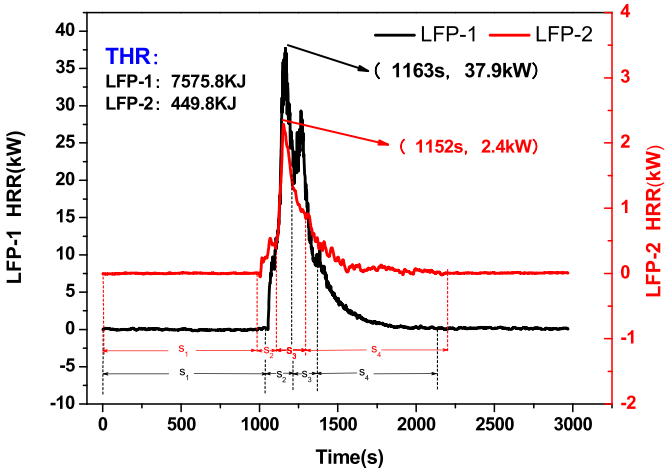

Fig. 6. HRR variations for cells at different combustion states.

Table 2
Detailed information about heat release rate of LIBs in different combustion states.

	SOC(%)	Peak HRR, kW	THR, kJ
LFP-1r	100	37.9	7575.8
LFP-2	100	2.4	449.8

Table 3
Calculation of heat release at each stage.

		S1	S2	S3	S4
Heat release(kJ)	LFP-1	0	2682.8(35.4%)	3231.1(42.6%)	1661.9(22.0%)
	LFP-2	0	32.1(7.1%)	260.2(57.8%)	157.5(35.0%)
Duration (**s**)	LFP-1	1059	136	179	805
	LFP-2	985	116	201	848

by poisonous gas [31]; hence, the toxicity must be assessed. The lethal concentration of CO is 1000 mg/m^3 [32], and the toxicity of HF at the same mass concentration is approximately 2.5 times that of CO. The comprehensive toxicity evaluation model is as follows [33]:

$$X_{FEC}=\frac{[HCl]}{F_{HCl}}+\frac{[HBr]}{F_{HBr}}+\frac{[HF]}{F_{HF}}+\frac{[SO_2]}{F_{SO_2}}+\frac{[NO_2]}{F_{NO_2}}+\frac{[acrolein]}{F_{acrolein}}+\frac{[formaldehyde]}{F_{formaldehyde}}+\sum\frac{[irri\ \tan\ t]}{F_{C_i}} \quad (1)$$

(X_{FEC}: Toxic gas effective concentration fraction; [i]: Concentration of each irritating gas; Fi: Critical concentration of each irritant gas that is expected to seriously compromise occupants' tenability.)

The larger is the value of X_{FEC}, the more toxic is the experimental gas. The X_{FEC} value of 1 indicates that the concentration of toxic gas is approximately the lethal concentration for humans. The calculation of gas production and toxicity is shown in Table 4. The X_{FEC} values of the two cells in the 6.48-m^3 combustion chamber are 3.53 and 5.38. Obviously the LFP-2 gas is more toxic than the LFP-1 gas. In practical applications, the toxicity can be higher in a small space.

In addition, in practical applications, LFP-2 can accumulate a large amount of pre-mixed combustible gas in a small space, which presents a deflagration hazard [34]. LFP-2 is more dangerous and destructive than LFP-1.

3.5. Material calorific value analysis

After disassembling the battery in the glove box, the mass ratio of each component of the new battery was calculated. The mass of the electrolyte was obtained through data subtraction. An oxygen bomb calorimeter was used to measure the combustion heat of the positive and negative materials, separator, electrolyte, and mixture of these. The results are shown in Table 5.

The combustion heat of the negative electrode material and diaphragm is the highest, and that of the positive electrode material is the lowest. The proportion of the mixed combustion of the electrolyte and negative electrode material considerably influences battery THR. THR is the highest when the electrolyte completely reacts with the negative electrode material.

The data in Table 5 can be used to calculate theoretical THR for complete combustion of a cell. If theoretical THR of the cell is set to Q, the resulting formula is as follows [35]:

$$Q=mQ_{(c,e)}+nQ_{(a,e)}+oQ_{(e)}+(1-m)Q_{(c,e)}+(1-n)Q_{(a)}+Q_{(g)} \quad (2)$$

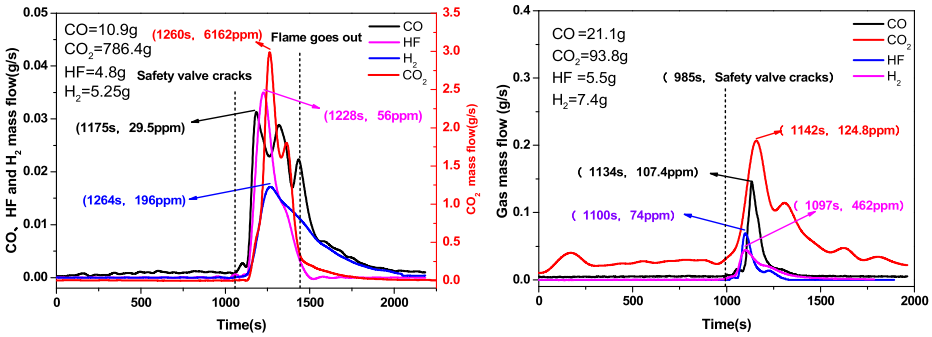

Fig. 7. Gas variations for cells at different combustion states.

Table 4
Detailed information about gas production and toxicity in different combustion states.

	Gas	LFP-1	LFP-2
Mass(g)	CO	10.9	21.1
	HF	4.8	5.5
	CO_2	786.4	93.8
	H_2	5.25	7.4
XFEC		3.53	5.38

where m, n, and o are the ratio parameters; $Q_{(x,y)}$ is the heat of combustion of each material and its mixture.

From calculation: $Q_{max} = 22110.97$ KJ; $Q_{min} = 20409.14$ KJ.

The complete combustion of a 60-Ah lithium iron phosphate battery releases 20409.14–22110.97 kJ energy.

The burned battery cell was ground and smashed, and the combustion heat value of mixed materials was measured to obtain the residual energy (ignoring the nonflammable battery casing and tabs) [35]. The calculation results are shown in Table 6.

The energy release of the cell during the experiment can be divided into three parts: P1 (HRR), P2 (internal anaerobic reaction exothermic heat; heat diffusion of the flue gas and battery), and P3 (residual energy). The total energy of the battery was calculated as an average value of 21260.06 kJ. P2 was obtained by subtracting P1 and P3 from the total energy. The calculation results are shown in Table 7.

The energy release of LFP-1 and LFP-2 in P2 are approximately 20%, indicating that the energy release in P2 does not affect the combustion state of the battery (Table 7). The external flame has no effect on anaerobic reaction heat release and ISC heat generation inside the battery. LFP-2 is 543.5 kJ more than LFP-1 in P2 due to the thermal diffusion of a large amount of the high-temperature gas.

P1 and P3 are substantially affected by the combustion state. After the experiment, most energy in the waste battery was not released, and the proportion of P3 was as high as 75.8% under the smouldering state.

After the voltage dropped to 0 V, the internal materials of the battery could still burn in the oxygen environment. Therefore, a battery that loses electrical performance cannot be considered safe [36]. Fire separation measures should be taken when storing these batteries.

4. Conclusions

In this study, several combustion tests were conducted on the large-format prismatic LIBs (LFP) with different combustion states. Battery TR was triggered using the heating plate. The fire behaviours, temperature, voltage variations, HRR, gas, and material calorific value were analysed. The main conclusions drawn are as follows:

1) The TR process under different combustion states is similar. The change trend of the flame intensity of LFP-1 during combustion is the same as that of the smoke production rate of LFP-2 during the smouldering process.
2) The temperature change trends of LFP-1 and LFP-2 are similar. The highest surface temperatures are 323 and 331.4 °C, and the highest heating rates are 1.64 °C/s and 1.71 °C/s, indicating that the combustion states does not affect the severity of the internal TR of the battery.
3) In terms of hazard, LFP-1 has a higher thermal hazard than LFP-2, and its THR is approximately 17 times that of LFP-2; LFP-2 has a higher gas hazard than LFP-1, and the concentration of the toxic gas in this experimental platform can reach 5.38 times the lethal concentration. In practical applications, LFP-2 can accumulate a large amount of premixed combustible gas in a small space, which presents a deflagration hazard. In poor-ventilation states, LFP-2 can be more dangerous and destructive than LFP-1.
4) During the experiment, the HRR and remaining energy of the battery were considerably affected by the combustion state.

Table 5
Battery calorific value test record table.

SOC (%)		100
Mass (g)	Total battery mass	1847
	Shell	324.3
	Current collector	266.1
Cathode material: Anode material: Electrolyte: Separator		6.70 : 5.69 : 3.66 : 1
Calorific value (kJ/g)	Cathode material	2.76
	Anode material	30.74
	Electrolyte	14.54
	Separator	30.34
	Cathode material + electrolyte	7.00
	Anode material + electrolyte	26.71

Table 6
Mass loss and calorific value before and after the experiment.

		LFP-1	LFP-2
Mass (g)	Before the experiment	1854	1851
	After the experiment	1487	1499
	Mass loss	367	352
	Battery wreckage	1162.7	1174.7
Combustion heat value of mixed materials (kJ/g)		8.18	13.70
Residual energy of the mixed material (kJ)		9510.89	16093.39

Table 7
Battery energy analysis during the experiment.

	P1 (kJ)	P2 (kJ)	P3 (kJ)
LFP-1	7575.8 (35.6%)	4173.37 (19.7%)	9510.89 (44.7%)
LFP-2	449.8 (2.1%)	4716.87 (22.1%)	16093.39 (75.8%)

After the test, most energy was not released, and the proportion of energy remaining under the smouldering states was as high as 75.8%. The internal materials of the battery could still burn in the oxygen environment. Therefore, fire sources should be avoided and fire prevention measures should be taken when storing these batteries.

CRediT authorship contribution statement

Q.I. Peiyan: Investigation, Conceptualization, Methodology, Formal analysis, Writing – original draft, Data curation. **Zhang Ming Jie:** Reviewing and Editing, Methodology. **Jiang Da:** Reviewing and Editing, Conduction of the experiments. **Yang Kai:** Supervision, Visualization, Funding acquisition. **Li Jianling:** Conceptualization, Methodology, Writing – review & editing, Supervision, Visualization, Funding acquisition. **Lai Yilin:** Validation, Reviewing and Editing, Methodology. **Gao Fei:** Reviewing and Editing, Resources. **Liu Hao:** Writing – review & editing, Validation, All authors reviewed the manuscript.

Declaration of competing interest

The authors declare that they have no known competing financial interests or personal relationships that could have appeared to influence the work reported in this paper.

Acknowledgments

This study is supported by the National Key Research and Development Program of China (No. 2019YFE0100200)

References

[1] Gao F, Zhu YL, Chuang QI, et al. Excitation source analysis of lithium ion batteries safety accidents. Chin J Power Sources 2019;43(3):99–103.
[2] Wang Q, Ping P, Zhao X, et al. ChemInform abstract: thermal runaway caused fire and explosion of lithium ion battery. J Power Sources 2012;208(24):210–24.
[3] Feng X, Zheng S, Ren D, et al. Investigating the thermal runaway mechanisms of lithium-ion batteries based on thermal analysis database. Appl Energy 2019;246(JUL.15):53–64.
[4] Feng X, Sun J, Ouyang M, et al. Characterization of penetration induced thermal runaway propagation process within a large format lithium ion battery module. J Power Sources 2015;275:261–73.
[5] Spotnitz RFJ. Abuse behavior of high-power, lithium-ion cells. J Power Sources 2003;113(1):81–100.
[6] Yang H, Bang H, Amine K, et al. Investigations of the exothermic reactions of natural graphite anode for Li-ion batteries during thermal runaway. J Electrochem Soc 2005;152(1):A73–9.
[7] Kawamura T, Kimura A, Egashira M, et al. Thermal stability of alkyl carbonate mixed-solvent electrolytes for lithium ion cells. J Power Sources 2002;104(2):260–4.
[8] Botte GG, White RE, Zhang Z. Thermal stability of LiPF 6–EC:EMC electrolyte for lithium ion batteries. J Power Sources 2001;97(none):570–5.
[9] Gachot Gg, P Ribiere Mathiron D, Grugeon S, Armand M, Leriche J-B, et al. Gas chromatography/mass spectrometry as a suitable tool for the Li-ion battery electrolyte degradation mechanisms study. Anal Chem 2011;83(2):478–85.
[10] Joachin H, Kaun TD, Zaghib K, et al. Electrochemical and thermal studies of carbon-coated LiFePO4 cathode. J Electrochem Soc 2009;156(6):A401–6.
[11] Yang H, Shen XD. Dynamic TGA–FTIR studies on the thermal stability of lithium/graphite with electrolyte in lithium-ion cell. J Power Sources 2007;167(2):515–9.
[12] Larsson F, Bertilsson S, Furlani M, et al. Gas explosions and thermal runaways during external heating abuse of commercial lithium-ion graphite-LiCoO2 cells at different levels of ageing. J Power Sources 2018;373(JAN.1):220–31.
[13] Xie H, Sun J, Jigang LI, et al. Research of leaked toxics from Li-ion battery electrical heat triggering thermal runaway. Energy.Storage. Sci. Technol 2019;44(6):90–6.
[14] Zhang Y, Wang H, Li W, et al. Quantitative identification of emissions from abused prismatic Ni-rich lithium-ion batteries. eTransportation 2019;2:100031.
[15] Li W, Rao S, Xiao Y, et al. Theoretical analysis of the fire boundaries of lithium-ion cell eruption gases caused by thermal runaway according to the thermal ignition theory. iScience 2021;24(5):102401.
[16] Huang P, Wang Q, Li K, et al. The combustion behavior of large scale lithium titanate battery. Sci Rep 2015;5(1):2419–30.
[17] Ping P, Wang QS, Huang PF, et al. Study of the fire behavior of high-energy lithium-ion batteries with full-scale burning test. J Power Sources 2015;285(jul.1):80–9.
[18] Wang S, Chen W, Chen G, et al. Study on combustion characteristics and fire risk of lithium ion battery. Electric Safety Technology 2019;275(3):44–50.
[19] Peng Y, Yang L, Ju X, et al. A comprehensive investigation on the thermal and toxic hazards of large format lithium-ion batteries with LiFePO_4 cathode. J Hazard Mater 2020;381(Jan.5):120916.1–120916.11.
[20] Fu Y, Lu S, Li K, et al. An experimental study on burning behaviors of 18650 lithium ion batteries using a cone calorimeter. J Power Sources 2015;273:216–22.
[21] Yu D, Li Y, Zhang S, et al. Fire risk analysis of lithium-ion batteries based on full scale test. Fire Sci Technol 2017;6(12):1731–4.
[22] Feng X, Zheng S, He X, et al. Time sequence map for interpreting the thermal runaway mechanism of lithium-ion batteries with LiNixCoyMnzO2 cathode. Frontiers.Energy. Res 2018;6.
[23] Liu Y, Tao F, Sun L, et al. Research of thermal runaway and internal evolution mechanism of lithium iron phosphate energy storage battery. High Volt Eng 2021;47(4):1333–43.
[24] Liu P, Liu C, Yang K, et al. Thermal runaway and fire behaviors of lithium iron phosphate battery induced by over heating. J Energy Storage 2020;31:101714.
[25] Wang Z, Ning X, Zhu K, et al. Evaluating the thermal failure risk of large-format lithium-ion batteries using a cone calorimeter. J Fire Sci 2019;37(1):81–95.
[26] Zhao L, Watanabe I, Doi T. TG-MS analysis of solid electrolyte interphase (SEI) on graphite negative-electrode in lithium-ion batteries. J Power Sources 2006;161(2):1275–80.
[27] Gnanaraj JS, Zinigrad E, Asraf L, et al. The use of accelerating rate calorimetry (ARC) for the study of the thermal reactions of Li-ion battery electrolyte solutions. J Power Sources 2003;119(Jun):794–8.
[28] Yang H, Shen XD. Dynamic TGA–FTIR studies on the thermal stability of lithium/graphite with electrolyte in lithium-ion cell. J Power Sources 2007;167(2):515–9.
[29] Wang Q, Sun J, Yao X, et al. Thermal stability of LiPF6/EC+DEC electrolyte with charged electrodes for lithium ion batteries. Thermochim Acta 2005;437(1–2):12–6.
[30] Gachot G, Grugeon S, Eshetu GG, Mathiron D, Ribière P, Armand M, et al. Thermal behaviour of the lithiated-graphite/electrolyte interface through GC/MS analysis. Electrochim Acta 2012;83(none):402–9.
[31] Zhao J, Zhu MX. Poisonous gas in fog of fire. Chin J Dis Control Prev 2003;7(4):338–40.
[32] Sun J, Qiu XP, Lai XK. Investigation on the toxic leakage production process of Li-ion battery induced by combustion[R]. Chengdu: Presentation at 8th China-US Electric Vehicle and Battery Technology Workshop; 2013.
[33] Lecocq A, Eshetu GG, Grugeon S, et al. Scenario-based prediction of Li-ion

batteries fire-induced toxicity. J Power Sources 2016;316(Jun.1):197–206.
[34] Li W , Wang H , Zhang Y , et al. Flammability characteristics of the battery vent gas: a case of NCA and LFP lithium-ion batteries during external heating abuse [J]. J Energy Storage, 24.
[35] Zhang MJ, Zhang J, Yang K, et al. Energy released during thermal runaway of lithium iron phosphate battery. Chin J Power Sources 2020;44(11):1583–6.
[36] Zhuo P, Zhao-Peng NI, Yang K, et al. Preliminary study on fire risk of lithium iron phosphate square cell under heat. Fire Sci Technol 2019;38(2):280–3.